



OPEN

Thermohydraulic analysis of covalent and noncovalent functionalized graphene nanoplatelets in circular tube fitted with turbulators

Hai Tao^{1,2,3}, Omer A. Alawi⁴, Omar A. Hussein⁵, Waqar Ahmed⁶, Ali H. Abdelrazek⁶, Raad Z. Homod⁷, Mahmoud Eltaweel⁸, Mayadah W. Falah⁹, Nadhir Al-Ansari¹⁰ & Zaher Mundher Yaseen¹¹✉

Covalent and non-covalent nanofluids were tested inside a circular tube fitted with twisted tape inserts with 45° and 90° helix angles. Reynolds number was $7000 \leq Re \leq 17,000$, and thermophysical properties were assessed at 308 K. The physical model was solved numerically via a two-equation eddy-viscosity model (SST k- ω turbulence). GNPs-SDBS@DW and GNPs-COOH@DW nanofluids with concentrations (0.025 wt.%, 0.05 wt.% and 0.1 wt.%) were considered in this study. The twisted pipes' walls were heated under a constant temperature of 330 K. The current study considered six parameters: outlet temperature, heat transfer coefficient, average Nusselt number, friction factor, pressure loss, and performance evaluation criterion. In both cases (45° and 90° helix angles), GNPs-SDBS@DW nanofluids presented higher thermohydraulic performance than GNPs-COOH@DW and increased by increasing the mass fractions such as 1.17 for 0.025 wt.%, 1.19 for 0.05 wt.% and 1.26 for 0.1 wt.%. Meanwhile, in both cases (45° and 90° helix angles), the value of thermohydraulic performance using GNPs-COOH@DW was 1.02 for 0.025 wt.%, 1.05 for 0.05 wt.% and 1.02 for 0.1 wt.%.

List of symbols

Ag	Silver
Al ₂ O ₃	Aluminum oxide
A _s	Surface area of tube (m ²)
CMC	Carboxymethyl cellulose
COOH	Carboxylic acid
C _p	Specific heat capacity (J/kg·K)
Cu	Copper
CuO	Copper oxide
D _h	Tube hydraulic diameter (mm)
DTTI	Dimpled twisted turbulator insert

¹College of Artificial Intelligence, Nanchang Institute of Science and Technology, Nanchang, China. ²School of Computer and Information, Qiannan Normal University for Nationalities, Duyun, Guizhou 558000, China. ³Institute for Big Data Analytics and Artificial Intelligence (IBDAAI), Universiti Teknologi MARA, 40450 Shah Alam, Selangor, Malaysia. ⁴Department of Thermofluids, School of Mechanical Engineering, Universiti Teknologi Malaysia (UTM), Skudai, 81310 Johor Bahru, Malaysia. ⁵Petroleum system control engineering department, College of Petroleum Processes Engineering, Tikrit University, Tikrit, Iraq. ⁶Takasago i-Kohza, Malaysia-Japan International Institute of Technology, Universiti Teknologi Malaysia, Kuala Lumpur, Malaysia. ⁷Department of Oil and Gas Engineering, Basrah University for Oil and Gas, Basrah, Iraq. ⁸School of Physics, Engineering and Computer Science, University of Hertfordshire, Hatfield AL10 9AB, UK. ⁹Building and construction techniques engineering department, AL-Mustaqbal University College, Hillah 51001, Iraq. ¹⁰Civil, Environmental and Natural Resources Engineering, Lulea University of Technology, 97187 Lulea, Sweden. ¹¹Civil and Environmental Engineering Department, King Fahd University of Petroleum and Minerals, Dhahran 31261, Saudi Arabia. ✉email: z.yaseen@kfupm.edu.sa

DW	Distilled water
f	Friction factor
Fe	Iron
FVM	Finite volume method
GNPs	Graphene nanoplatelets
GO	Graphene oxide
Gr	Graphene
H/D	Twisted tape ratio
H ₂ SO ₄	Sulfuric acid
HNO ₃	Nitric acid
h_{tc}	Heat transfer coefficient (W/m ² . K)
k	Thermal conductivity (W/m-K)
k_{eff}	Effective thermal conductivity (W/m K)
L	Tube length (mm)
\dot{m}	Mass flow rate (kg/s)
MgO	Magnesium oxide
MWCNTs	Multi-walled carbon nanotubes
Nu_{avg}	Average Nusselt number
PCM	Phase change material
PEC	Performance assessment criteria
Pr	Prandtl number
Pt	Platinum
Q_{gain}	Heat gain (W)
Re	Reynolds number
SDBS	Sodium dodecylbenzenesulfonate
SST	Spiky twisted tapes
T_f	Bulk temperature (K)
THNF	Tripartite hybrid nanofluids
T_{in}	Inlet fluid temperature (K)
TiO ₂	Titanium dioxide
T_{out}	Outlet fluid temperature (K)
T_w	Wall surface temperature (K)
v	Working fluid velocity (m/s)
VcTT	V-cuts twisted tape
WC	Wire coil
wt.%	Weight concentration of nanoparticles
ΔP	Pressure drop (Pa)
ϵ	Energy dissipation rate (m ² /s ³)
μ	Dynamic viscosity (Ns/m ²)
ρ	Density (kg/m ³)

Study background knowledge and motivation. Heat exchangers are thermal devices used to transport heat during cooling and heating operations¹. Heat exchanger thermohydraulic performance increases heat transfer coefficients and lowers working fluid resistance. Some heat transfer enhancement techniques have been developed, including turbulence promoters^{2–11} and nanofluids^{12–15}. Due to its simplicity of maintenance and low cost, twisted tape insertion is one of the most successful ways of enhancing heat transfer in a heat exchanger^{7,16}.

Implemented literature review on nanofluids-based twisted pipes. In a series of experimental and computational research, the hydrothermal characteristics of a mixture of nanofluids and a heat exchanger with twisted tape inserts were investigated. Experimental work explored the hydrothermal properties of three different metallic nanofluids (Ag@DW, Fe@DW, and Cu@DW) within a heat exchanger with spiky twisted tapes (STT)¹⁷. The heat transfer coefficient of STT has gone up 11 and 67% compared to the basic pipe. The SST arrangement was the best cost-efficient based on the performance factor, with the parameters of $\alpha = \beta = 0.33$. Furthermore, n increase of 18.2% was observed using Ag@DW, even though the largest increase in pressure loss was just 8.5%. The heat transfer and pressure loss physical characteristics in a concentric tube with and without wire coil (WC) turbulators were explored using turbulent forced convection Al₂O₃@DW nanofluid flow¹⁸. Maximum average Nusselt number (Nu_{avg}) and pressure loss were seen under the $Re = 20,000$ when the pitch wire coil = 25 mm and 1.6 volume%-Al₂O₃@DW nanofluids. Laboratory studies were also carried out to investigate the heat transfer and pressure loss features of graphene oxide (GO@DW) nanofluids flowing through a basic circular tube with WC inserts¹⁹. According to the results, 0.12 volume%-GO@DW raised the convective heat transfer coefficient by about 77%. An additional experimental study developed (TiO₂@DW) nanofluid, examining thermo-hydraulic performances of dimpled tubes fitted having twisted tape inserts²⁰. The greatest thermo-hydraulic efficiency of 1.258 was achieved using 0.15 volume%-TiO₂@DW in a tilted 45°-dimple and embedded with a twisted tape ratio of 3.0. Single-phase and two-phase (mixed) simulation models solved the CuO@DW nanofluid flow and heat transfer in the various solid concentrations (1–4% volume%)²¹. The maximum thermal efficiency in a tube with one twisted tape insertion was 2.18, but it was 2.04 in a tube with two twisted tape insertions on the same terms (two-phase model, $Re = 36,000$ and 4 volume%). The non-Newtonian

turbulent nanofluid flow of Carboxymethyl cellulose (CMC) and Copper oxide (CuO) was examined in a basic pipe and a pipe having twisted insertions²². Nu_{avg} demonstrated improvements like 16.1% (for basic pipe) and 60% [for a twisted pipe with a ratio of $(H/D=5)$]. Frequently, the smaller twisted tape ratio has established a higher friction factor. An experimental study examined the influences of pipe having twisted tape (TT) and wire coil (WC) on the heat transfer and friction factor properties using CuO@DW nanofluid²³. Using 0.3volume%-CuO@DW at $Re=20,000$ enhanced the heat transfer up to its maximum value of 44.45% in a WC-2 tube. Furthermore, by applying twisted tape and wire coil insertions under the same boundary conditions, the friction factors increased by 1.17-times and 1.19-times compared to DW. In general, the thermal performance factor of nanofluids with wire coil insertions was better than for twisted tape insertions. The overall performance of turbulent (MWCNTs@DW) nanofluid flow was examined inside a horizontal pipe with coiled wire inserted²⁴. All cases had a thermal performance parameter > 1 , indicating that combining nanofluids with wire coil insertions improved heat transfer without consuming pumping power. Experiments under turbulent $Al_2O_3 + TiO_2@DW$ nanofluid flow conditions were carried out on hydrothermal properties in a double-tube heat exchanger having various modified V-cuts twisted tape (VcTT) insertions²⁵. Nu_{avg} was enhanced significantly by the percentage of 132%, and the friction factor was up to 55% when compared to DW in a basic pipe. Also, the exergetic effectiveness of nanocomposite $Al_2O_3 + TiO_2@DW$ was discussed within a double pipe heat exchanger²⁶. They found in their research that employing $Al_2O_3 + TiO_2@DW$ and TT increased the exergy efficiency relative to DW. In a concentric tube heat exchanger having a VcTT turbulator, Singh and Sarkar²⁷ used phase change material (PCM) dispersed mono/nanocomposite nanofluids ($Al_2O_3@DW$ with PCM and $Al_2O_3 + PCM$). They reported that heat transfer and pressure loss increased when the twisting ratio decreased and nanoparticle concentration increased. More heat transfer and pressure loss were achieved with a larger V-cut depth ratio or a lower width ratio. Furthermore, graphene-platinum (Gr-Pt) was applied to examine the thermal, frictional, and total entropy production rates in tubes having 2-TT insertions²⁸. Their study noted that less percentage of (Gr-Pt) significantly decreased the thermal entropy formation than relatively increased frictional entropy development. $Al_2O_3@MgO$ hybrid nanofluid and tapered WC can be regarded as a good mix because of the enhanced $(h/\Delta p)$ ratio to improve the hydrothermal properties of a double pipe heat exchanger²⁹. A numerical model was used to solve the exergo-economic environmental effectiveness of heat exchanger having various tripartite hybrid nanofluids (THNF) ($Al_2O_3 + Graphene + MWCNTs$) suspended in DW³⁰. The combination of dimpled twisted turbulator insert (DTTI) and ($Al_2O_3 + Graphene + MWCNTs$) was desired because its performance assessment criteria (PEC) was in the range of 1.42–2.35.

Research objectives. So far, very little attention has been paid to the role of covalent and non-covalent functionalization on hydraulic flow in thermal fluids. The specific objective of this study was to compare the thermal-hydraulic performance of (GNPs-SDBS@DW) and (GNPs-COOH@DW) nanofluids within twisted tape inserts with 45-degree and 90-degree helix angles. The thermophysical properties were measured at $T_{in} = 308$ K. Meanwhile, three mass fractions were taken into consideration during the comparison such as (0.025 wt.%, 0.05 wt.% and 0.1 wt.%). The shear stress transport (SST $k-\omega$) model in three-dimensional turbulence was used to solve the thermohydraulic performance. As a result, by proving Thermal-Hydraulic Performance and Optimization the practical working fluids in such engineering systems, this study offers a significant contribution to research on the positive properties (heat transfer) and negative properties (frictional pressure drop).

Numerical methodologies

Physical model and numerical method. The base configuration is a smooth pipe ($L=900$ mm and $D_h=20$ mm). The twisted tapes were inserted with the dimensions of (length=20 mm, thickness=0.5 mm, and profile=30 mm). Meanwhile, the helical profile length, width, and path were 20 mm, 0.5 mm, and 30 mm. The twisted tape was tilted at an angle of 45° and 90°. Different working fluids such as DW, non-covalent nanofluids (GNPs-SDBS@DW), and covalent nanofluids (GNPs-COOH@DW) were tested inside the heat exchangers at $T_{in} = 308$ K, three different mass concentrations, and different Reynolds numbers. The outer walls of the spiral pipes were heated at a constant surface temperature of 330 K to examine the heat transfer enhancement parameters.

Figure 1 illustrates a schematic design of the twisted tape insertion pipe with the applicable boundary conditions and grid domains. As noted, velocity and pressure boundary conditions are applied at the inlet and exit parts of the spiral pipes. The non-slip condition is applied to the pipe wall under the constant surface temperature. The pressure-based solution was used in the current numerical simulations. Meanwhile, (ANSYS FLUENT 2020R1) program was used to convert the partial differential equations (PDEs) into a system of algebraic equations using the finite volume method (FVM). The second-order SIMPLE (Semi-Implicit Method for Pressure Linked Equations-Consistent) methodology correlates the velocity–pressure. It should be emphasized that convergence for the residual of mass, momentum, and energy equations is less than 10^3 and 10^6 , respectively.

Assumptions and mathematical formulas. The homogeneous model is used to explain the nature of nanofluids. A continuous fluid with excellent thermophysical properties is formed by adding nanomaterials to the base fluid (DW). In this regard, the temperature and velocity of the base fluid and nanomaterials have the same values. The effective single-phase flow works due to the abovementioned theories and hypotheses in this research. Several examinations have confirmed the single-phase technique's validity and applicability for nanofluid flow^{31,32}.

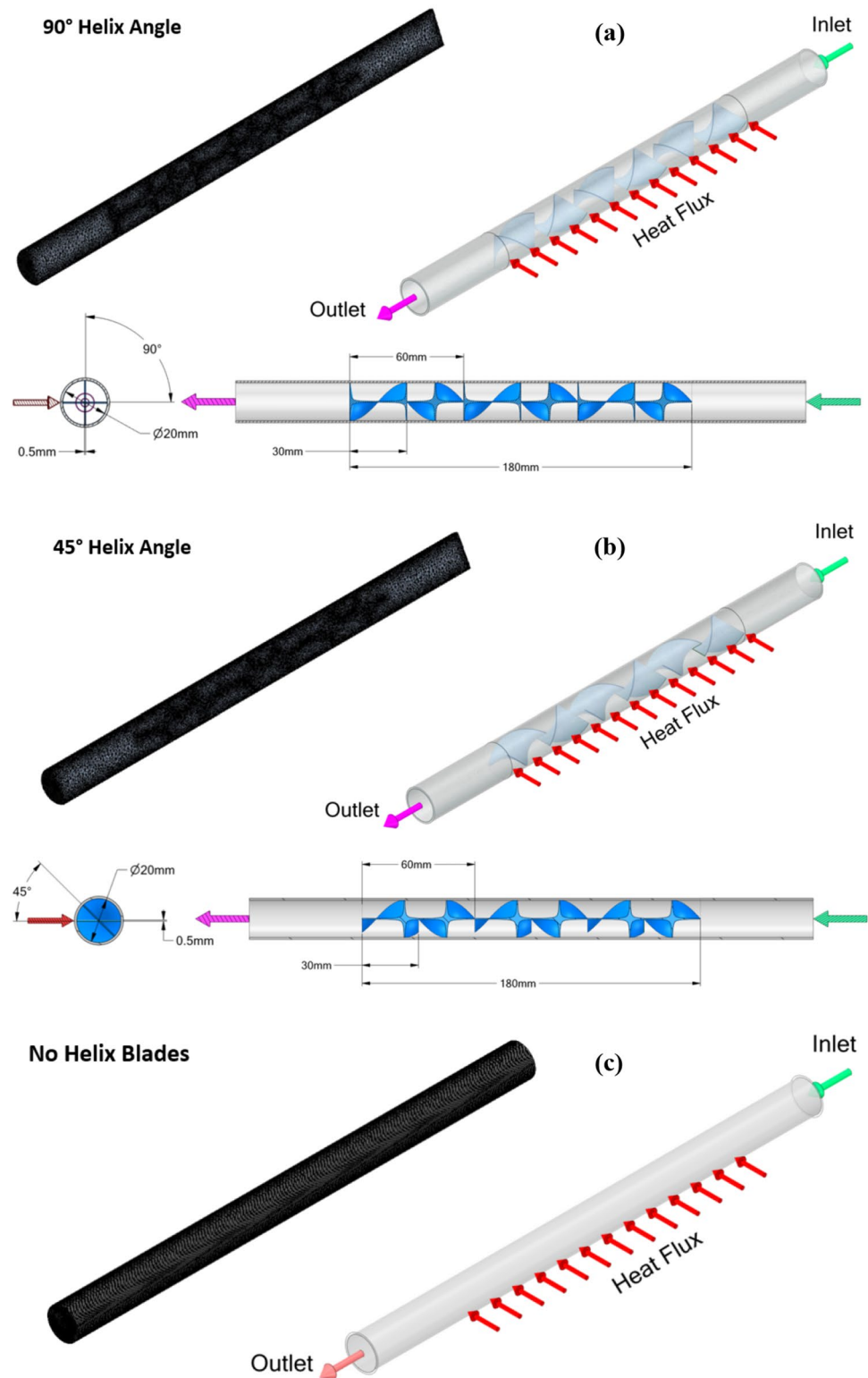


Figure 1. Schematic diagram of physical and computational domain; (a) 90° helix angle, (b) 45° helix angle, (c) no helix blades.

The flow of nanofluids is supposed to be Newtonian turbulent, incompressible, and steady-state. Compression work and viscous heating are not significant in this investigation. Also, the thicknesses of the inner and outer pipe walls are not considered. Therefore, the mass, momentum, and energy conservation governing equations of the thermal model may be stated as follows³³:

Thermophysical properties	DW	SDBS-GNPs@DW			COOH-GNPs@DW		
		0.025 wt.%	0.05 wt.%	0.1 wt.%	0.025 wt.%	0.05 wt.%	0.1 wt.%
ρ (kg/m ³)	994.1	995.1151	996.8895	998.158	994.9564	995.9241	996.8885
c_p (J/kg·K)	4178	4152.66	4104.075	4055.95	4164.51	4111.11	4056.685
k (W/m·K)	0.623	0.645	0.675	0.695	0.685	0.71	0.754
μ (Ns/m ²)	0.0007	0.001	0.0011	0.0013	0.0008	0.0009	0.0009

Table 1. Thermal-physical properties of DW, (SDBS-GNPs@DW) and (COOH-GNPs@DW) nanofluids³⁴.

Governing equation for mass

$$\nabla \cdot (\rho \vec{V}) = 0 \quad (1)$$

Governing equation for momentum

$$\nabla \cdot (\rho \vec{V} \vec{V}) = -\nabla P + \nabla \cdot \left((u + u_t) (\nabla \vec{V} + \nabla \vec{V}^T) \right) + \rho \vec{g} \quad (2)$$

Governing equation for energy transport

$$\nabla \cdot (\rho C_p \vec{V}) = \nabla \cdot (k_{eff} \nabla T) + \rho \epsilon \quad (3)$$

where \vec{V} is the mean velocity vector, $K_{eff} = K + K_i$ is the effective thermal conductivity of covalent and non-covalent nanofluids, and ϵ is the energy dissipation rate. The effective thermo-physical properties of the nanofluid, including density (ρ), viscosity (μ), specific heat capacity (C_p), and thermal conductivity (k) as measured in experimental study³⁴ for a temperature of 308 K, as listed in Table 1 were used in these simulations.

The turbulent nanofluid flow in plain and TT pipes was numerically simulated at the Reynolds numbers condition of $7000 \leq Re \leq 17,000$. These simulation cases and the convective heat transfer coefficient were analyzed by applying the Mentor Shear Stress Transport (SST) κ - ω turbulence model, a two-equation Reynolds-averaged Navier–Stokes turbulence model that is commonly used for aerodynamic research. Moreover, this model operates with no wall functions and is accurate near-wall^{35,36}. The (SST) κ - ω turbulence model governing equations are as follows:

Kinematic Eddy viscosity

$$\nu_T = \frac{a_1 k}{\max(a_1 \omega, SF_2)} \quad (4)$$

Turbulence kinetic energy

$$\frac{\partial k}{\partial t} + U_j \frac{\partial k}{\partial x_j} = P_k - \beta^* k \omega + \frac{\partial}{\partial x_j} \left((v + \sigma_k \nu_T) \frac{\partial k}{\partial x_j} \right) \quad (5)$$

Specific dissipation rate

$$\frac{\partial \omega}{\partial t} + U_j \frac{\partial \omega}{\partial x_j} = \alpha S^2 - \beta \omega^2 + \frac{\partial}{\partial x_j} \left((v + \sigma_\omega \nu_T) \frac{\partial \omega}{\partial x_j} \right) + 2(1 - F_1) \sigma_\omega^2 \frac{1}{\omega} \frac{\partial k}{\partial x_i} \frac{\partial \omega}{\partial x_i} \quad (6)$$

Closure coefficients and auxiliary relations

$$F_2 = \tanh \left(\max \left(\frac{2\sqrt{k}}{\beta^* \omega y}, \frac{500\nu}{y^2 \omega} \right)^2 \right) \quad (7)$$

$$P_k = \min \left(\tau_{ij} \frac{\partial U_i}{\partial x_j}, 10\beta^* k \omega \right) \quad (8)$$

$$F_1 = \tanh \left(\left(\min \left(\max \left(\frac{2\sqrt{k}}{\beta^* \omega y}, \frac{500\nu}{y^2 \omega} \right), \frac{4\sigma_\omega^2 k}{CD_{k\omega} y^2} \right) \right)^4 \right) \quad (9)$$

$$CD_{k\omega} = \max \left(2\rho \sigma_\omega^2 \frac{1}{\omega} \frac{\partial k}{\partial x_i} \frac{\partial \omega}{\partial x_i}, 10^{-10} \right) \quad (10)$$

$$\phi = \phi_1 F_1 + \phi_2 (1 - F_1) \quad (11)$$

$$\alpha_1 = \frac{5}{9}, \alpha_2 = 0.44$$

$$\beta_1 = \frac{3}{40}, \beta_2 = 0.0828 \quad (12)$$

$$\beta^* = \frac{9}{100}$$

$$\sigma_{k_1} = 0.85, \sigma_{k_2} = 1$$

$$\sigma_{\omega_1} = 0.5, \sigma_{\omega_2} = 0.856$$

where S is the strain rate magnitude and y is the distance to the next surface. Meanwhile, $\alpha_1, \alpha_2, \beta_1, \beta_2, \beta^*, \sigma_{k_1}, \sigma_{k_2}, \sigma_{\omega_1}$ and σ_{ω_2} represent all model constants. F_1 and F_2 refer to the blending functions. Note: $F_1 = 1$ inside the boundary layer and 0 in the free stream.

Performance evaluation parameters are used to examine turbulent convective heat transfer, covalent and non-covalent nanofluid flow, such as³¹:

Reynolds number

$$Re = \frac{\rho v D_h}{\mu} \quad (13)$$

Prandtl number

$$Pr = \frac{\mu C_p}{k} \quad (14)$$

Heat gain (W)

$$Q_{Gain} = \dot{m} \times C_p \times (T_{out} - T_{in}) \quad (15)$$

Heat transfer coefficient (W/m². K)

$$h_{tc} = \frac{Q_{Gain}}{A_s \times (\bar{T}_w - \bar{T}_f)} \quad (16)$$

Average Nusselt number

$$Nu_{avg} = \frac{h_{tc} D_h}{k} \quad (17)$$

Friction factor

$$f = \frac{2 \times \Delta P \times D_h}{\rho \times v^2 \times L} \quad (18)$$

Pressure loss

$$\Delta P = P_{in} - P_{out} \quad (19)$$

Dittus–Boelter equation

$$Nu_{avg} = 0.023 \times Re^{0.8} \times Pr^{0.4} \quad (20)$$

Petukhov equations

$$Nu_{avg} = \frac{\left(\frac{f}{8}\right) Re Pr}{1.07 + 12.7 \left(\frac{f}{8}\right)^{1/2} (Pr^{2/3} - 1)} \quad (21)$$

$$f = (0.78 \ln Re - 1.64)^{-2}$$

Gnielinski equation

$$Nu_{avg} = \frac{\left(\frac{f}{8}\right) (Re - 1000) Pr}{1 + 12.7 \left(\frac{f}{8}\right)^{1/2} (Pr^{2/3} - 1)} \quad (22)$$

Notter-Rouse equation

$$Nu_{avg} = 5 + 0.015 \times Re^{0.856} \times Pr^{0.347} \quad (23)$$

Blasius equation

$$f = \frac{0.3164}{Re^{0.25}} \quad (24)$$

Thermohydraulic performance

$$PEC = \frac{Nu_{NFs}}{Nu_{DW}} / \left(\frac{f_{NFs}}{f_{DW}} \right)^{1/3} = \frac{Nu_{45^\circ, 90^\circ}}{Nu_{Plain}} / \left(\frac{f_{45^\circ, 90^\circ}}{f_{Plain}} \right)^{1/3}. \quad (25)$$

In this regard, (ρ) , (v) , (D_h) and (μ) are used for the density, working fluid velocity, hydraulic diameter, and dynamic viscosity. (C_p) and (k) are the specific heat capacity and thermal conductivity of the flowing fluid. Also, (\dot{m}) refer to the mass flow rate and $(T_{out} - T_{in})$ symbolizes the outlet/inlet temperature difference. (NFs) refer to the covalent, non-covalent nanofluids, and (DW) refer to the distilled water (base fluid). $A_s = \pi DL$, $\bar{T}_f = \frac{(T_{out} - T_{in})}{2}$ and $\bar{T}_w = \sum \frac{T_w}{n}$.

Thermal-physical properties of covalent and non-covalent nanofluids

The thermal-physical properties of base fluid (DW), non-covalent nanofluids (GNPs-SDBS@DW), and covalent nanofluids (GNPs-COOH@DW) were collected from the published literature (experimental study) under $T_{in} = 308$ K, as shown in Table 1³⁴. In a typical experiment, to produce a non-covalent (GNP-SDBS@DW) nanofluid with known mass percentages, a certain gram of pristine GNPs was initially weighted via digital balance. A weight ratio SDBS/pristine GNPs of (0.5:1) suspended in DW. Meanwhile, the covalent (COOH-GNPs@DW) nanofluids were synthesized using a strong acid medium of HNO_3 and H_2SO_4 in the volume ratio of (1:3) to add carboxyl groups at the surface of GNPs. The covalent and non-covalent nanofluids were suspended in DW with three different mass percentages, such as 0.025 wt.%, 0.05 wt.% and 0.1 wt.%.

Results and discussion

Verification of the numerical outputs. Grid independence tests were run on four different computational domains to ensure grid size did not affect the simulations. In the case of 45° twisted pipe, the number of elements was 249,033 for element size of 1.75 mm, 307,969 for element size of 2 mm, 421,406 for element size of 2.25 mm, and 564,940 for element size of 2.5 mm, respectively. Moreover, the number of elements in the instance of a 90° twisted pipe was 245,531 for element size of 1.75 mm, 311,584 for element size of 2 mm, 422,708 for element size of 2.25 mm, and 573,826 for element size of 2.5 mm, respectively. The accuracy of thermal properties such as (T_{out}) , (h_{tc}) , and (Nu_{avg}) readings increased by decreasing the number of elements. Meanwhile, the accuracy of friction factor and pressure drop values showed a completely different behavior (Fig. 2). Grid (2) was employed as the main mesh domain to evaluate thermohydraulic performance in the simulation cases.

The current numerical results were verified using well-known empirical correlations and equations such as Dittus-Boelter, Petukhov, Gnielinski, Notter-Rouse, and Blasius for heat transfer and friction factor properties. The comparison was under the condition of $7000 \leq Re \leq 17,000$. As per Fig. 3, the average and maximum errors between the simulation results and heat transfer equations were 4.050% and 5.490% (Dittus-Boelter), 9.736% and 11.33% (Petukhov), 4.007% and 7.483% (Gnielinski), and 3.883% and 4.937% (Notter-Rouse). Meanwhile, the average and maximum errors between the simulation results and friction factor equations were 7.346% and 8.039% (Blasius) and 8.117% and 9.002% (Petukhov).

Thermohydraulic enhancement of nanofluids/basefluids. This section discusses the thermohydraulic properties of non-covalent (GNPs-SDBS) and covalent (GNPs-COOH) based water nanofluids at three various mass fractions and Reynolds number as an average with respect to base fluid (DW). Two geometries twisted taped heat exchangers with (45° and 90° helix angles) were discussed in $7000 \leq Re \leq 17,000$. Figure 4 shows the average outlet temperature of nanofluids to base fluid (DW) $\left(\frac{T_{out NFs}}{T_{out DW}} \right)$ at (0.025 wt.%, 0.05 wt.% and 0.1 wt.%). $\left(\frac{T_{out NFs}}{T_{out DW}} \right)$ is always less than 1, meaning that the outlet temperature of non-covalent (GNPs-SDBS) and covalent (GNPs-COOH) nanofluids was less than the outlet temperature for base fluid. The lowest and highest decrease was achieved by 0.1 wt.-%-COOH@GNPs and 0.1 wt.-%-SDBS@GNPs, respectively. This phenomenon is caused by an increase in the Reynolds number at the constant weight fraction, which causes a change in nanofluid characteristics (i.e., density and dynamic viscosity).

Figures 5 and 6 depict the average heat transfer properties of nanofluids to base fluid (DW) at (0.025 wt.%, 0.05 wt.% and 0.1 wt.%). The average heat transfer properties are always greater than one, meaning that the heat transfer properties of non-covalent (GNPs-SDBS) and covalent (GNPs-COOH) nanofluids were enhanced relative to the base fluid. The lowest and highest enhancement was achieved by 0.1 wt.-%-COOH@GNPs and 0.1 wt.-%-SDBS@GNPs, respectively. Heat transport properties improved when the Reynolds number increased due to greater fluid mixing and turbulence in tube¹. The liquid running through the small gaps gets a higher velocity, causing velocity/thermal boundary layers to thin, thus, enhancing the heat transfer rate. Adding more nanoparticle percentages to the base fluid exhibits positive and negative outcomes. The favorable influences include increased nanoparticle collision, fluid thermal conductivity, and beneficial requirements for heat transfer augmentation.

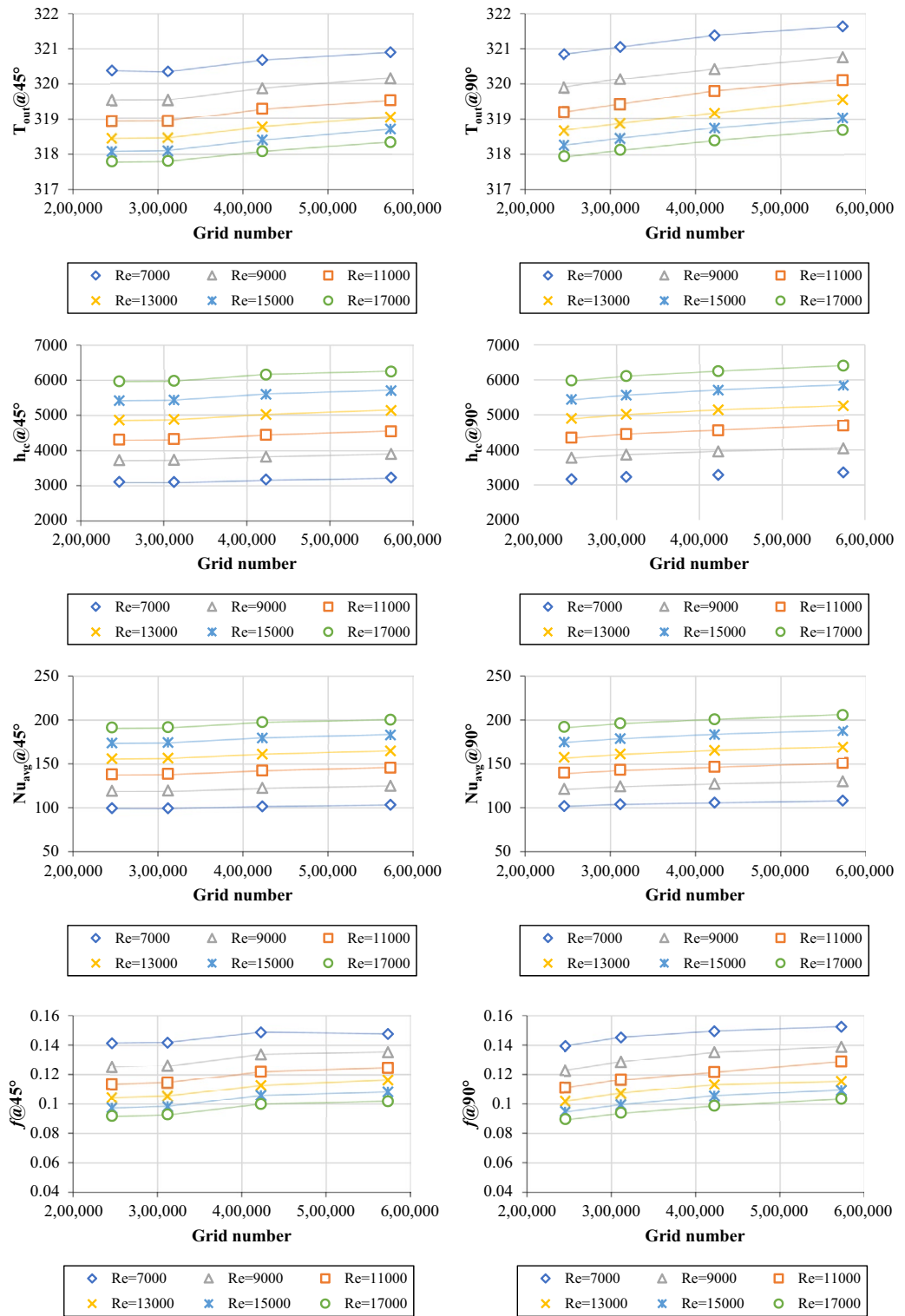


Figure 2. Grid independence tests for heat transfer and pressure drop properties using 45° and 90° twisted pipes for DW.

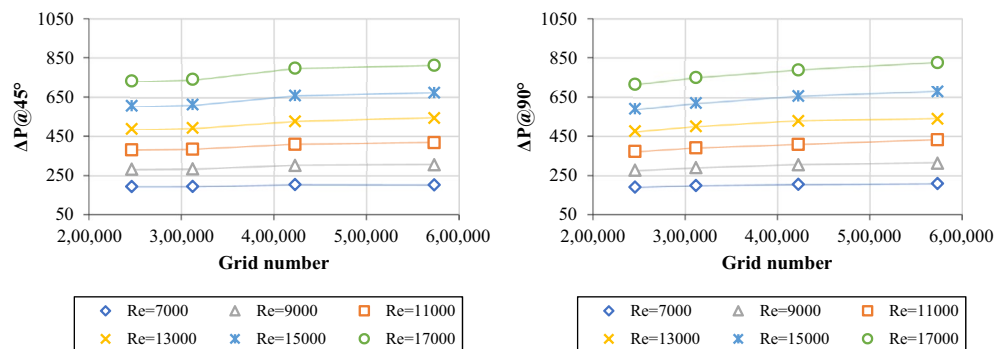


Figure 2. (continued)

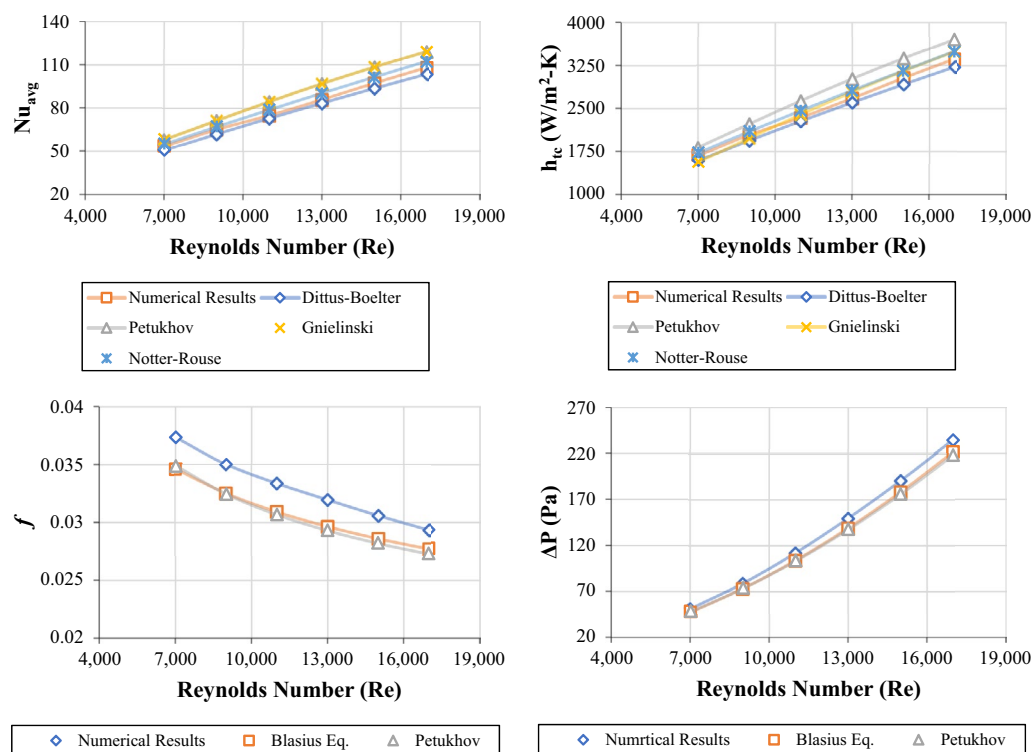


Figure 3. Heat transfer and fluid flow properties of DW at different Reynolds numbers using numerical calculations and empirical correlations.

Meanwhile, the negative impact is the increased dynamic viscosity of nanofluid, which decreases the movement of nanofluid and, therefore, the average Nusselt number (Nu_{avg}). The increased thermal conductivity of the (GNPs-SDBS@DW) and (GNPs-COOH@DW) nanofluids is supposed to be due to Brownian motion and micro-convection of graphene nanoparticles suspended in DW³⁷. (GNPs-COOH@DW) nanofluids had a higher thermal conductivity than (GNPs-SDBS@DW) nanofluids and distilled water. Adding more nanomaterial percentages to the base fluid increased their thermal conductivity (Table 1)³⁸.

Figure 7 explains the average friction factor of nanofluids to base fluid (DW) (f_{NFs}/f_{DW}) at the mass percentages of (0.025%, 0.05% and 0.1%). The average friction factor is always ≈ 1 , implying that the friction factor of non-covalent (GNPs-SDBS@DW) and covalent (GNPs-COOH@DW) nanofluids was the same with base fluid. The heat exchangers with less space created more flow obstruction and increased flow friction¹. Mainly, the friction factor increased marginally along with increasing nanofluid mass percentages. The higher friction loss was caused by increased nanofluid dynamic viscosity and shear stresses on surfaces with higher nano-graphene mass percentages in the base fluid. According to Table (1), the dynamic viscosity of the (GNPs-SDBS@DW) nanofluid was higher than that of the (GNPs-COOH@DW) nanofluid at equal weight percentages, because of the impact of adding surfactant during the production of non-covalent nanofluids.

Figure 8 shows the average pressure loss of nanofluids to base fluid (DW) ($\frac{\Delta P_{NFs}}{\Delta P_{DW}}$) at the mass percentages of (0.025%, 0.05% and 0.1%). Non-covalent (GNPs-SDBS@DW) nanofluids demonstrate higher average pressure

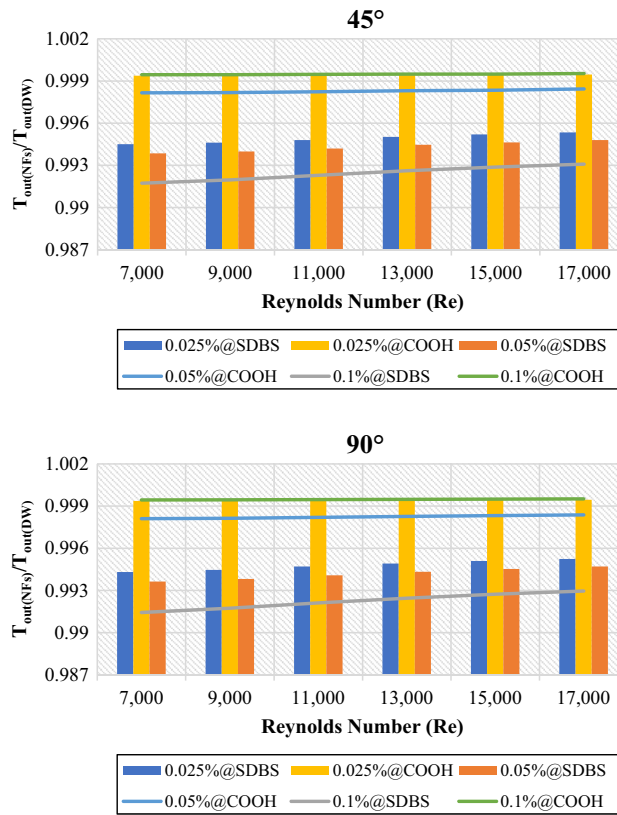


Figure 4. Outlet temperature of nanofluids to base fluid versus Reynolds numbers for 45° and 90° tubes.

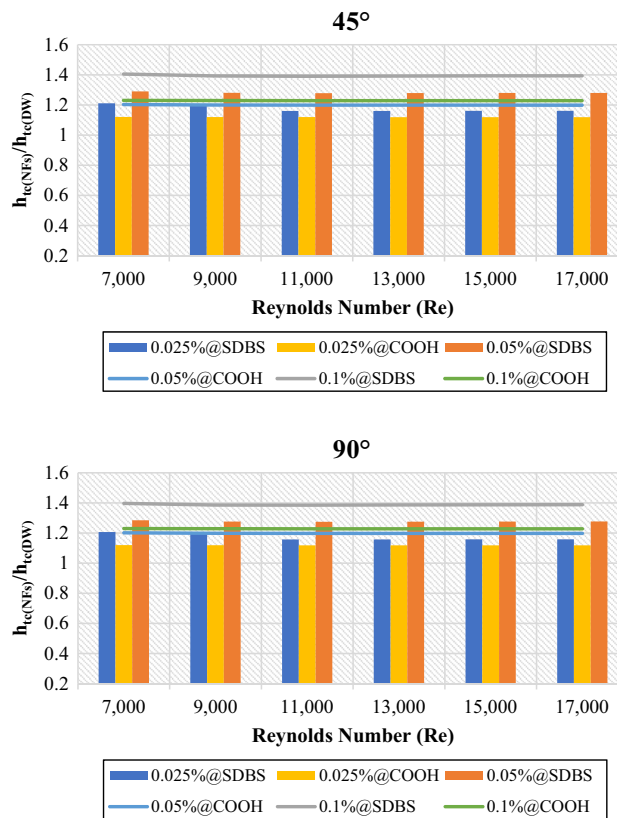


Figure 5. Heat transfer coefficient of nanofluids to base fluid versus Reynolds numbers for 45° and 90° tubes.

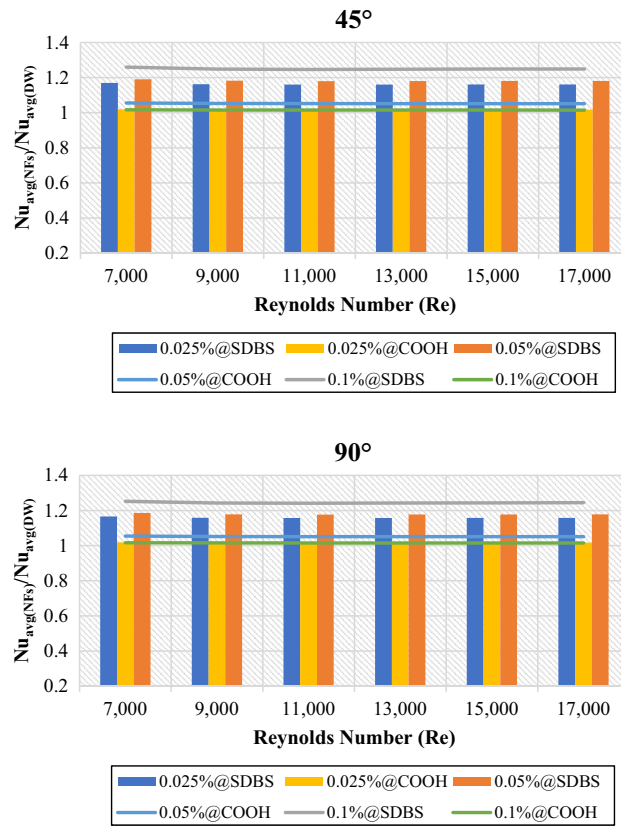


Figure 6. Average Nusselt number of nanofluids to base fluid versus Reynolds numbers for 45° and 90° tubes.

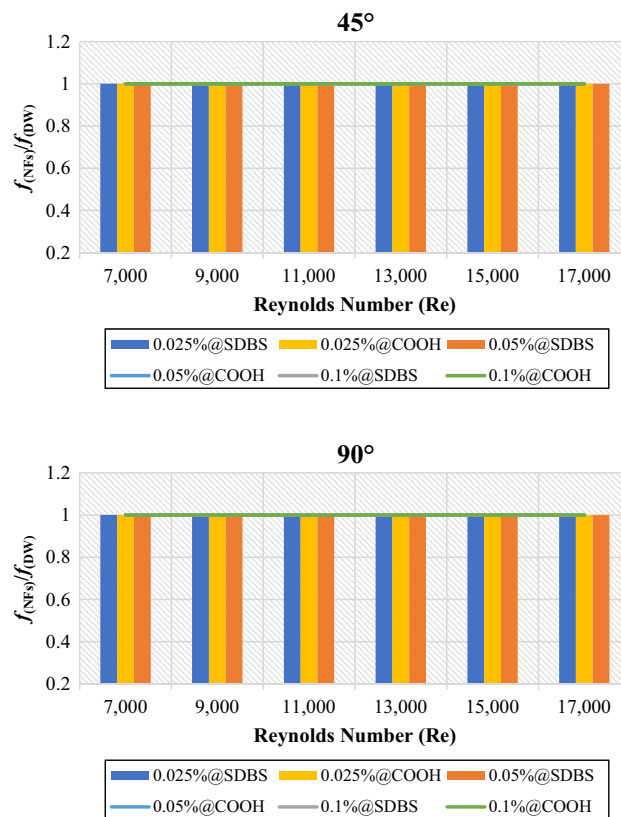


Figure 7. Friction factor of nanofluids to base fluid versus Reynolds numbers for 45° and 90° tubes.

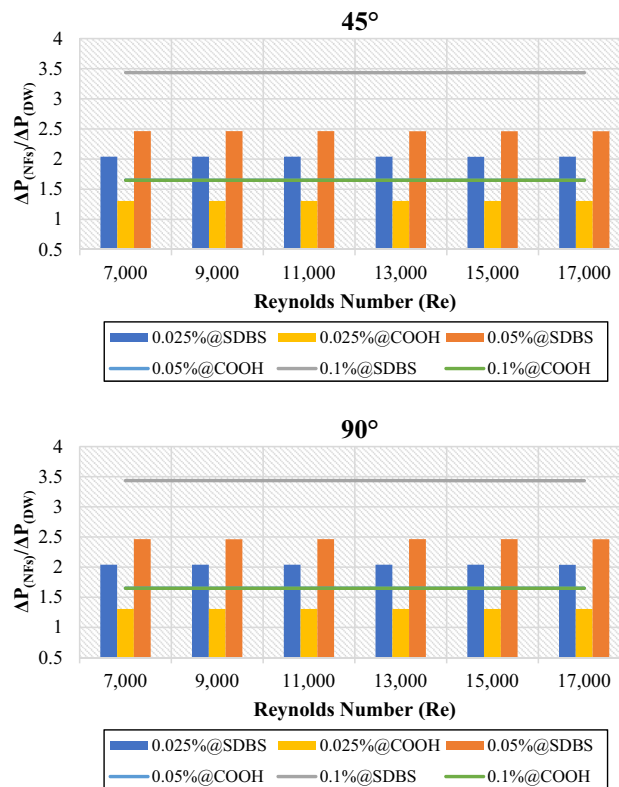


Figure 8. Pressure drops of nanofluids to base fluid versus Reynolds numbers for 45° and 90° tubes.

loss and increase by increasing the weight percentage to 2.04% for 0.025 wt.%, 2.46% for 0.05 wt.%, and 3.44% for 0.1 wt.% in both cases (45° and 90° helix angles). Meanwhile, (GNPs-COOH@DW) nanofluids exhibited lower average pressure loss, increasing from 1.31% for 0.025 wt.% to 1.65% for 0.05 wt.%. The average pressure loss for 0.05 wt.%-COOH@GNPs and 0.1 wt.%-COOH@GNPs is 1.65%. As shown, the pressure drop increased in all cases by the Re number increment. The increased pressure drop in high Re values could be justified by the direct relation with the volume flow rate. Therefore, higher Re numbers in tubes bring about a higher pressure drop, which calls for the increased pumping power^{39,40}. Moreover, higher pressure loss because of higher swirl and turbulence intensities produced by the larger surface area increased the interaction of pressure forces with inertial forces in the boundary layer¹.

Overall, the performance evaluation criterion (PEC) of non-covalent (GNPs-SDBS@DW) and covalent (GNPs-COOH@DW) nanofluids is shown in Fig. 9. (GNPs-SDBS@DW) nanofluids present higher PEC values than (GNPs-COOH@DW) in both cases (45° and 90° helix angles) and are raised by increasing the mass fractions such as 1.17 for 0.025 wt.%, 1.19 for 0.05 wt.% and 1.26 for 0.1 wt.%. Meanwhile, the value of PEC using (GNPs-COOH@DW) nanofluids is 1.02 for 0.025 wt.%, 1.05 for 0.05 wt.% and 1.02 for 0.1 wt.% in both cases (45° and 90° helix angles). Generally, as the Reynolds number increased, the thermohydraulic performance factor decreased considerably. The drop in thermohydraulic performance factor systematically is credited to the rise of (Nu_{Nfs}/Nu_{DW}) and the decrease of (f_{Nfs}/f_{DW}) as the Reynolds number increases¹.

Thermohydraulic enhancement of twisted pipe/plain pipe. This section discusses the thermohydraulic properties of water (DW), non-covalent (GNPs-SDBS@DW), and covalent (GNPs-COOH@DW) nanofluids at three different weight concentrations and Reynolds numbers. Two twisted taped heat exchanger geometries were considered with (45° and 90° helix angles) in the range of $7000 \leq Re \leq 17,000$ relatives to plain pipe to evaluate the average values of thermohydraulic properties. Figure 10 shows the outlet temperature of water and nanofluids as an average value using (45° and 90° helix angles) to the plain pipe ($\frac{T_{out Twisted}}{T_{out Plain}}$). The non-covalent (GNPs-SDBS@DW) and covalent (GNPs-COOH@DW) nanofluids were in three different mass fractions, such as 0.025 wt.%, 0.05 wt.% and 0.1 wt.%. As illustrated in Fig. 11, the average outlet temperature values ($\frac{T_{out Twisted}}{T_{out Plain}}$) are > 1 , indicating that the outlet temperature of (45° and 90° helix angles) heat exchangers was more significant than the value of outlet temperature for the plain pipe due to a more vigorous turbulence intensity and better fluid mixing. Furthermore, as the Reynolds number rises, the outlet temperature of DW, non-covalent, and covalent nanofluids declines. Based fluid (DW) has the highest average output temperature values. Meanwhile, the lowest value is dedicated for 0.1 wt.%-SDBS@GNPs. The non-covalent (GNPs-SDBS@DW) nanofluids show lower average outlet temperature relative to covalent (GNPs-COOH@DW) nanofluids. As the flow field is mixed up more as a result of the twisted tape, the wall heat flux can more easily pass through the fluid flow, raising the

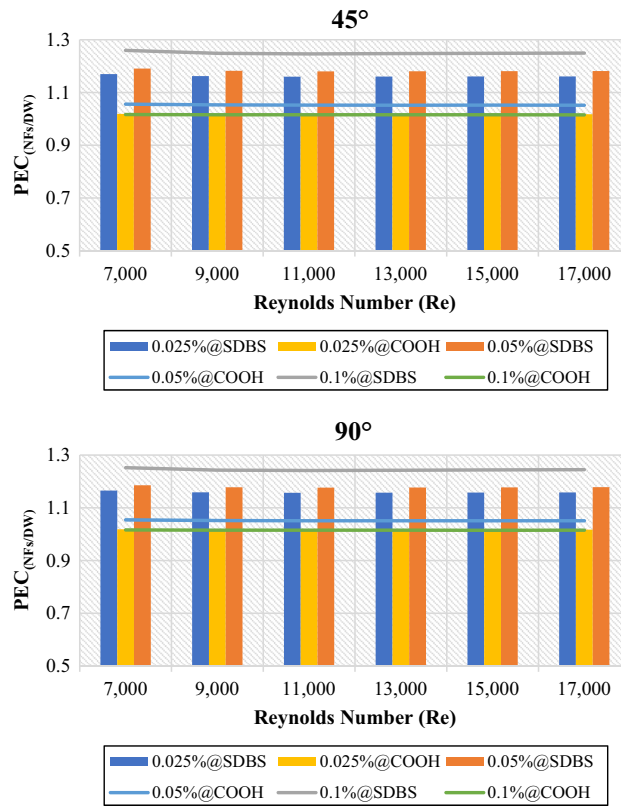


Figure 9. Hydrothermal performance of nanofluids to base fluid versus Reynolds numbers for 45° and 90° tubes.

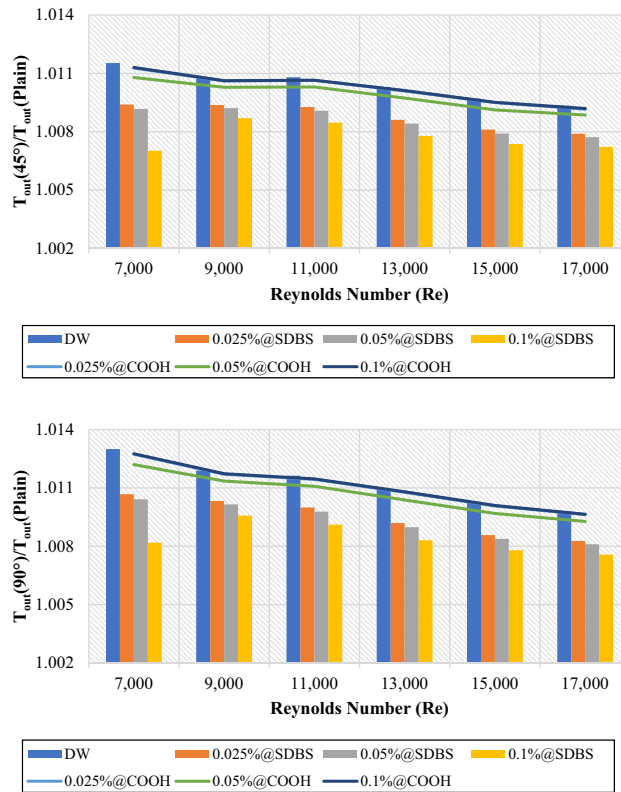


Figure 10. Outlet temperature of (45° and 90° helix angles) relative to plain pipe versus Reynolds numbers for different nanofluids.

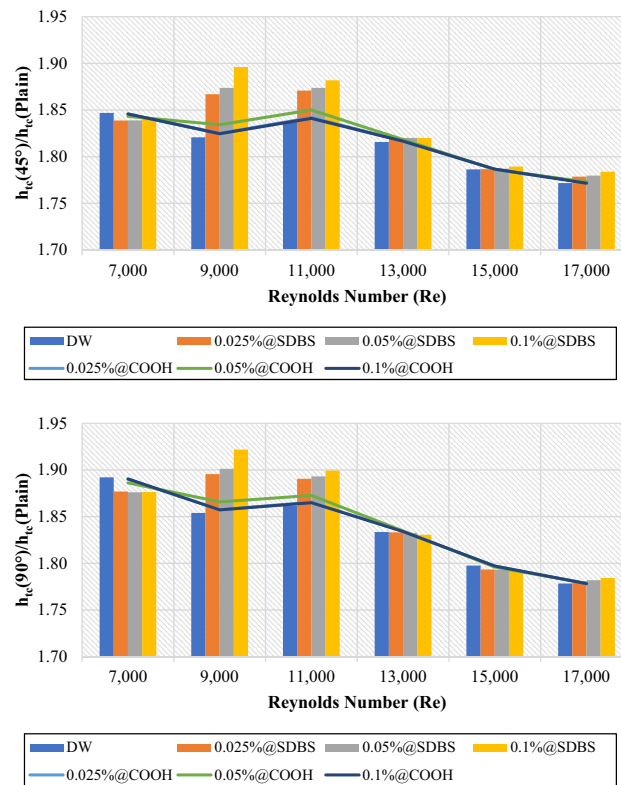


Figure 11. Heat transfer coefficient of (45° and 90° helix angles) relative to plain pipe versus Reynolds numbers for different nanofluids.

bulk temperature. Smaller twisted tape ratio values result in better penetration, which improves heat transmission. The twisted tape, on the other hand, is seen to maintain a lower temperature near the wall, which in turn raises Nu_{avg} . With twisted tape inserts, a higher Nu_{avg} indicates improved convective heat transmission across tube²². Increased residence time due to raised flow path with extra mixing and turbulence creation, they are resulting in a rise in the fluid's outlet temperature⁴¹.

The primary mechanisms of heat transfer enhancement owing to twisted tape are as follows: 1. The lowering of a heat transfer tube's hydraulic diameter generates an increase in flow velocity and curvature, which in turn increases shear stress near the wall and promotes secondary motion. 2. The velocity increases near the tube wall due to the blocked twisted tape, reducing the thickness of the boundary layer. 3. The helical flow following the twisted tape causes an increase in velocity. 4. Induced whirling flow improves fluid mixing between the core and near-wall flow areas⁴². Figures 11 and 12 showed the heat transfer properties such as (heat transfer coefficient and average Nusselt number) of DW and nanofluids as an average value using twisted tape inserts pipes relative to the plain pipe. The non-covalent (GNPs-SDBS@DW) and covalent (GNPs-COOH@DW) nanofluids were in three different mass fractions, such as 0.025 wt.%, 0.05 wt.% and 0.1 wt.%. In both heat exchangers (45° and 90° helix angles), the average values of heat transfer properties are > 1, which indicates improvement of heat transfer coefficient and average Nusselt number using twisted pipes relative to plain pipe. The non-covalent (GNPs-SDBS@DW) nanofluids show higher average heat transfer enhancement than covalent (GNPs-COOH@DW) nanofluids. The highest augmentation in the heat transfer properties was reached by 0.1 wt.%-SDBS@GNPs with the value of 1.90 in both heat exchangers (45° and 90° helix angles) at Re = 900. This means that the role of uniform TT in increasing turbulence intensity is far more major at the lower fluid velocities (Reynolds numbers)⁴³. The heat transfer coefficient and average Nusselt number in TT pipes are higher than in a plain pipe due to the induction of multiple swirl flows, resulting in thinner boundary layer. Comparison to the basic pipe (no twisted tape insertions), whether the existence of TT produces increased turbulence intensity, flow mixing of working fluids, and heat transfer enhancement²¹.

Figures 13 and 14 presented the average friction factor ($f_{Plain}^{Twisted}$) and pressure loss ($\frac{\Delta P_{Twisted}}{\Delta P_{Plain}}$) of 45° and 90° heat exchangers relative to the plain pipe using DW, (GNPs-SDBS@DW) and (GNPs-COOH@DW) nanofluids with (0.025 wt.%, 0.05 wt.%, and 0.1 wt.%). It can be observed from Figs. 13 and 14, as the Reynolds number increases in both heat exchangers (45° and 90° helix angles), the ratio of friction factor ($f_{Plain}^{Twisted}$) and pressure loss ($\frac{\Delta P_{Twisted}}{\Delta P_{Plain}}$) decreases. For all scenarios evaluated, the friction factor and pressure loss values are superior at lower Reynolds numbers. The average friction factor and pressure loss are between 3.78 and 3.12. The average friction factor and pressure loss show that the value of (45° and 90° helix angles) heat exchangers has risen three times than the plain pipe. Furthermore, by flowing higher working fluid velocity, the friction factor decreases.

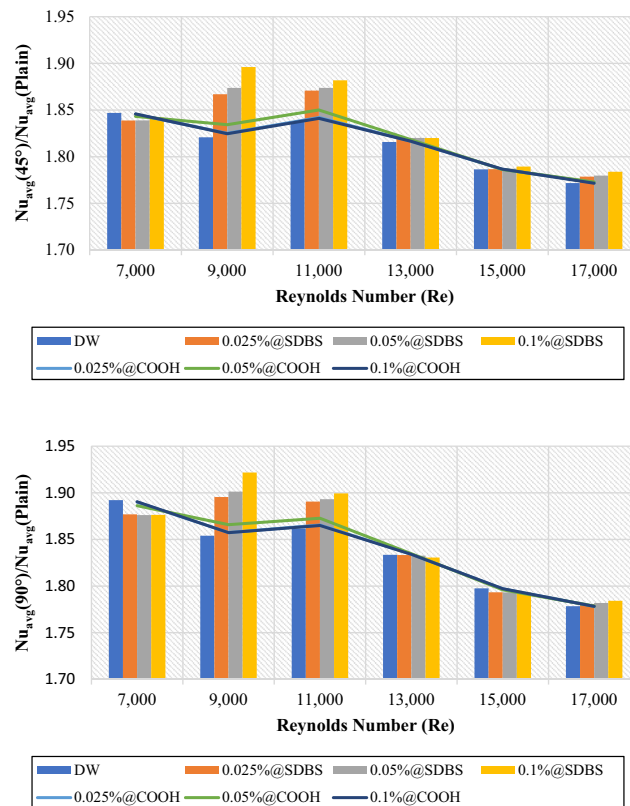


Figure 12. Average Nusselt number of (45° and 90° helix angles) relative to plain pipe versus Reynolds numbers for different nanofluids.

This problem is because, by raising the Reynolds number, the thickness of the boundary layer decreases, causing reducing in the influence of the affected area by dynamic viscosity and decreasing velocity gradient and shear stress, and, therefore, reducing the friction factor²¹. Improvement of the blocking effect because of the existence of TT and increased swirling flows produces a much higher-pressure loss for the non-uniform TT pipe than the basic ones. Additionally, for both the basic and TT pipes, it can be seen that the pressure drop is increasing by increasing the velocity of the working fluids⁴³.

Generally, Fig. 15 illustrates the performance evaluation criterion (PEC) of 45° and 90° heat exchangers relative to the plain pipe ($\frac{PEC_{Twisted}}{PEC_{Plain}}$) using DW, (GNPs-SDBS@DW) and covalent (GNPs-COOH@DW) nanofluids in (0.025 wt.%, 0.05 wt.%, and 0.1 wt.%). The value for the ($\frac{PEC_{Twisted}}{PEC_{Plain}}$) is > 1 in both instances (45° and 90° helix angles) heat exchangers. Furthermore, the better value of ($\frac{PEC_{Twisted}}{PEC_{Plain}}$) is reached at Re = 11,000. The 90°-degree angle heat exchanger revealed a modest increase ($\frac{PEC_{Twisted}}{PEC_{Plain}}$) values in comparison to the 45°-degree angle heat exchanger. Furthermore, at Re = 11,000, 0.1 wt.%-GNPs@SDBS indicates a higher ($\frac{PEC_{Twisted}}{PEC_{Plain}}$) value, such as 1.25 for 45°-degree angle heat exchanger and 1.27 for 90°-degree angle heat exchanger. It is larger than unity at all mass fraction percentages, pointing out that the pipe with twisted tape inserts outperforms the plain pipe. It is noted that heat transfer augmentation supplied by the tape inserts results in significantly increased friction loss²².

Velocity contours and streamlines. Appendix A displays the velocity streamlines of 45° and 90° heat exchangers that use the DW, 0.1 wt.%-GNPs-SDBS@DW, and 0.1 wt.%-GNPs-COOH@DW at Re = 7000. The streamlines in the transverse planes are the most remarkable features of the impact of the twisted tape inserts on the mainstream flow. The applications of 45° and 90° heat exchangers illustrated about the same velocity in the near-wall regions. Meanwhile, Appendix B illustrates the velocity contours of 45° and 90° heat exchangers using DW, 0.1 wt.%-GNPs-SDBS@DW, and 0.1 wt.%-GNPs-COOH@DW at Re = 7000. The velocity contours were at three separate locations (slices) such as Plain-1 (P1 = -30 mm), Plain-4 (P4 = 60 mm) and Plain-7 (P7 = 150 mm). The lowest velocity is near the pipe wall, and fluid velocity increases in the direction of the pipe center. Also, moving across the pipe increases the low-velocity zones next to the wall. This is because of the growth of hydrodynamic boundary layers, which increases the thickness of the low velocity zone next to the wall. Moreover, increasing the Reynolds number improves the total velocity level at all cross-sections, reducing the thickness of the low-velocity zones through pipe³⁹.

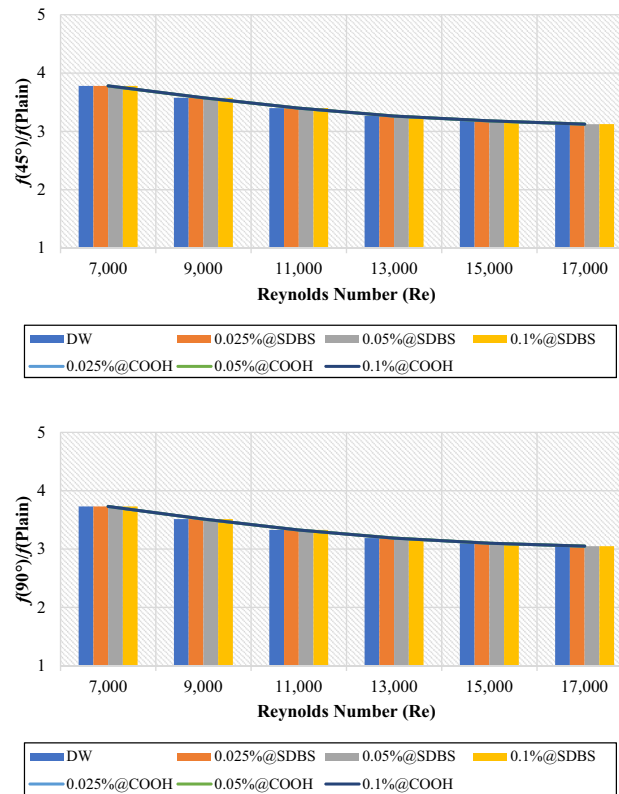


Figure 13. Friction factor of (45° and 90° helix angles) relative to plain pipe versus Reynolds numbers for different nanofluids.

Conclusions

Covalent and non-covalent functionalized Graphene nanoplatelets were evaluated inside twisted tape inserts with 45° and 90° helix angles. The heat exchangers were numerically solved via SST k-omega turbulence models in $7000 \leq Re \leq 17,000$. The thermophysical properties were calculated at $T_{in} = 308$ K. At the same time, the walls of the twisted pipe were heated under a constant temperature of 330 K. (GNPs-SDBS@DW) and (GNPs-COOH@DW) nanofluids in three mass dilutions such as (0.025 wt.%, 0.05 wt.% and 0.1 wt.%). Current research considers six principal factors: outlet temperature, heat transfer coefficient, average Nusselt number, friction factor, pressure loss, and performance evaluation criterion. The following are the key findings:

- i. The average outlet temperature ($T_{out\ Nanofluids}/T_{out\ Basefluid}$) is always less than 1, meaning that the outlet temperature of non-covalent (GNPs-SDBS@DW) and covalent (GNPs-COOH@DW) nanofluids was less than of outlet temperature for base fluid. Meanwhile, the average outlet temperature ($T_{out\ Twisted}/T_{out\ Plain}$) values are > 1 , indicating that the outlet temperature of (45° and 90° helix angles) was more substantial than the value of outlet temperature for the plain pipe.
- ii. In both cases, the average (Nanofluids/Basefluids) and (Twisted pipe/Plain pipe) of heat transfer properties always show > 1 . The non-covalent (GNPs-SDBS@DW) nanofluids showed higher average heat transfer augmentation corresponding to covalent (GNPs-COOH@DW) nanofluids.
- iii. The average friction factor ($f_{Nanofluids}/f_{Basefluid}$) of non-covalent (GNPs-SDBS@DW) and covalent (GNPs-COOH@DW) nanofluids is always ≈ 1 . Meanwhile, the average friction factor ($f_{Twisted}/f_{Plain}$) of non-covalent (GNPs-SDBS@DW) and covalent (GNPs-COOH@DW) nanofluids is always > 3 .
- iv. In both cases (45° and 90° helix angles), (GNPs-SDBS@DW) nanofluids showed higher ($\Delta P_{Nanofluids}/\Delta P_{Basefluid}$) as 2.04% for 0.025 wt.%, 2.46% for 0.05 wt.% and 3.44% for 0.1 wt.%. In the meantime, (GNPs-COOH@DW) nanofluids showed lower ($\Delta P_{Nanofluids}/\Delta P_{Basefluid}$) from 1.31% for 0.025 wt.% to 1.65% for 0.05 wt.%. Furthermore, the average pressure loss ($\Delta P_{Twisted}/\Delta P_{Plain}$) of non-covalent (GNPs-SDBS@DW) and covalent (GNPs-COOH@DW) nanofluids is always > 3 .
- v. In both cases (45° and 90° helix angles), (GNPs-SDBS@DW) nanofluids presented higher ($PEC_{Nanofluids}/PEC_{Basefluid}$) values than (GNPs-COOH@DW), such as 1.17 for 0.025 wt.%, 1.19 for 0.05 wt.% and 1.26 for 0.1 wt.%. Meanwhile, the value of ($PEC_{Nanofluids}/PEC_{Basefluid}$) using (GNPs-COOH@

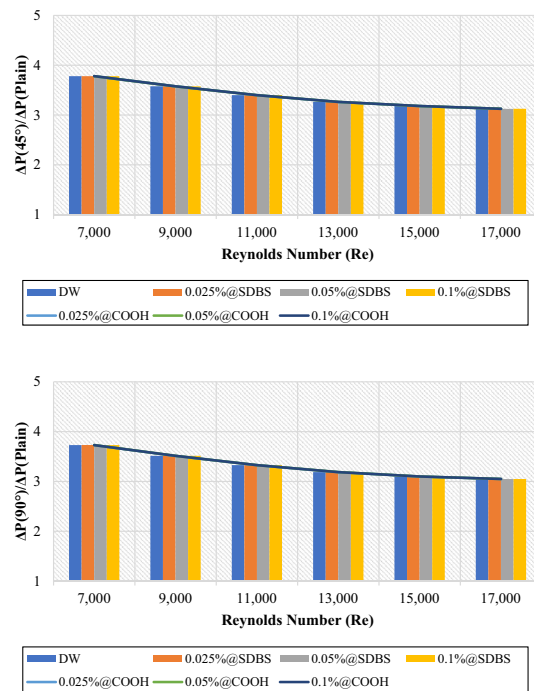


Figure 14. Pressure loss of (45° and 90° helix angles) relative to plain pipe versus Reynolds numbers for different nanofluids.

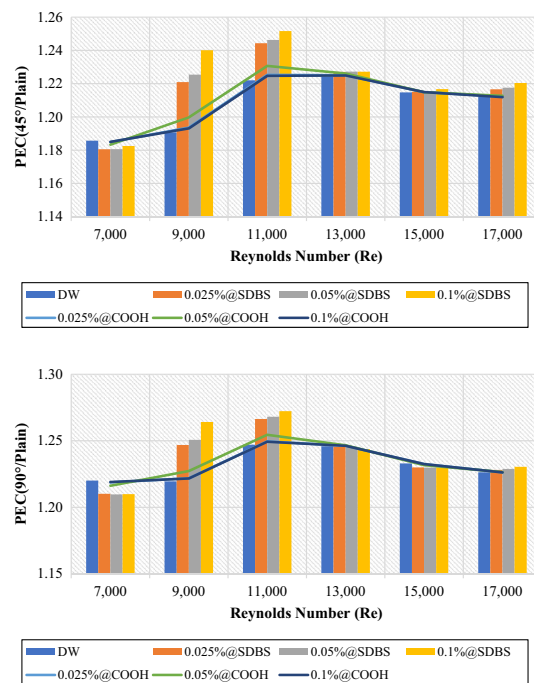


Figure 15. Performance evaluation criterion of (45° and 90° helix angles) relative to plain pipe versus Reynolds numbers for different nanofluids.

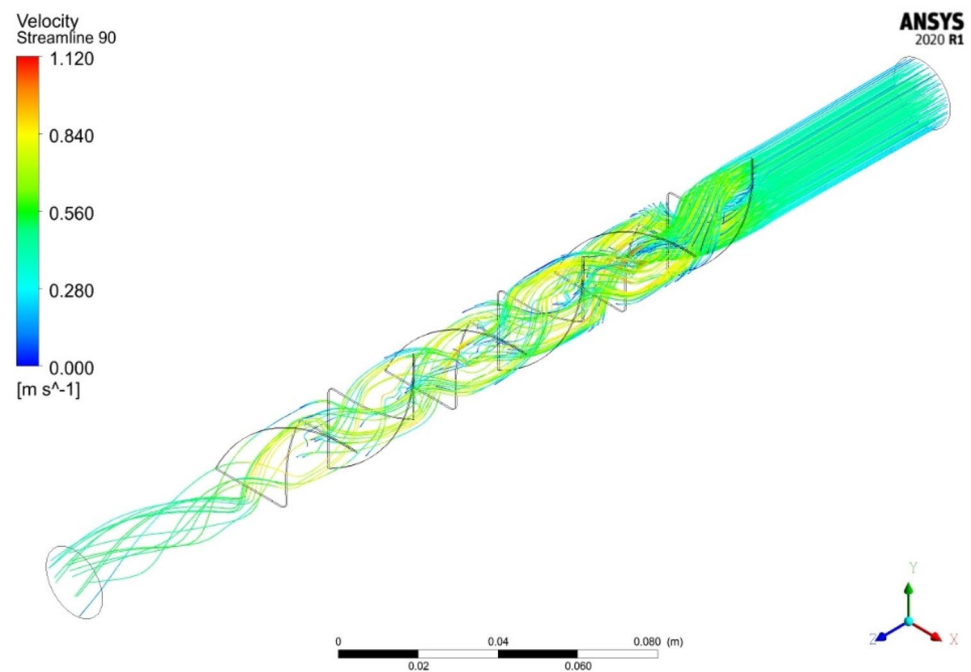
DW) nanofluids was 1.02 for 0.025 wt.%, 1.05 for 0.05 wt.% and 1.02 for 0.1 wt.%. Moreover, at $Re = 11,000$, 0.1 wt.-%-GNPs@SDBS shows the higher ($PEC_{Twisted}/PEC_{Plain}$) value, such as 1.25 for 45° helix angle and 1.27 for 90° helix angle.

Data availability

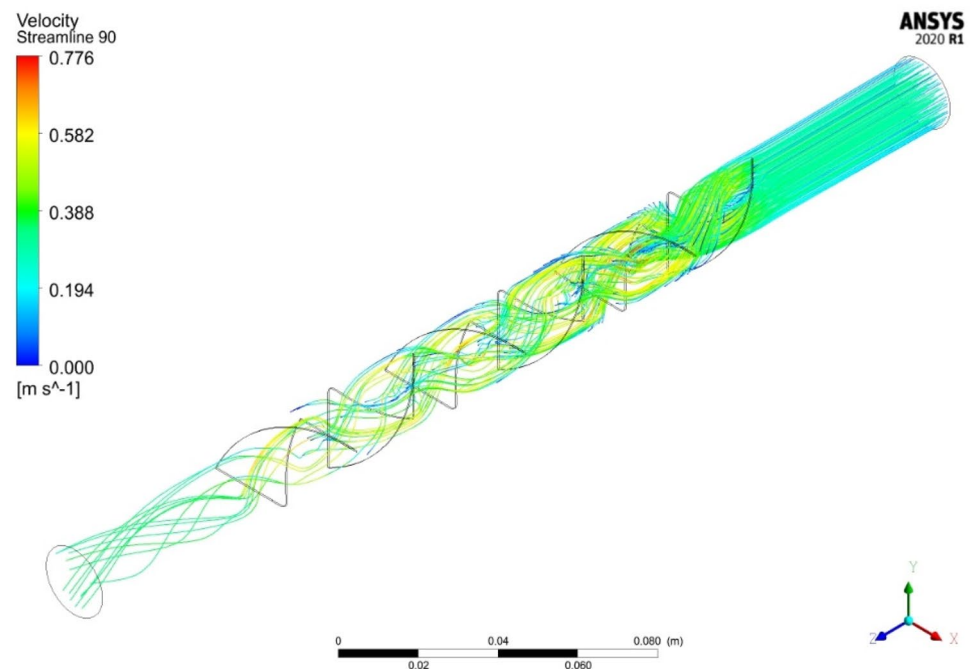
All the data generated or analyzed during the current study are included in this published article.

Appendix A

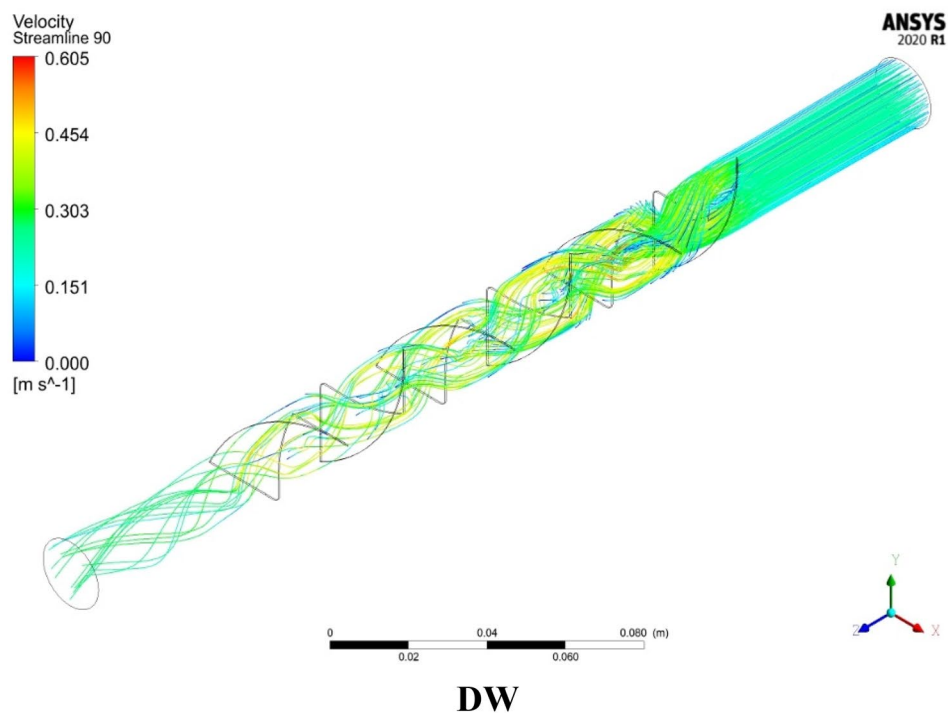
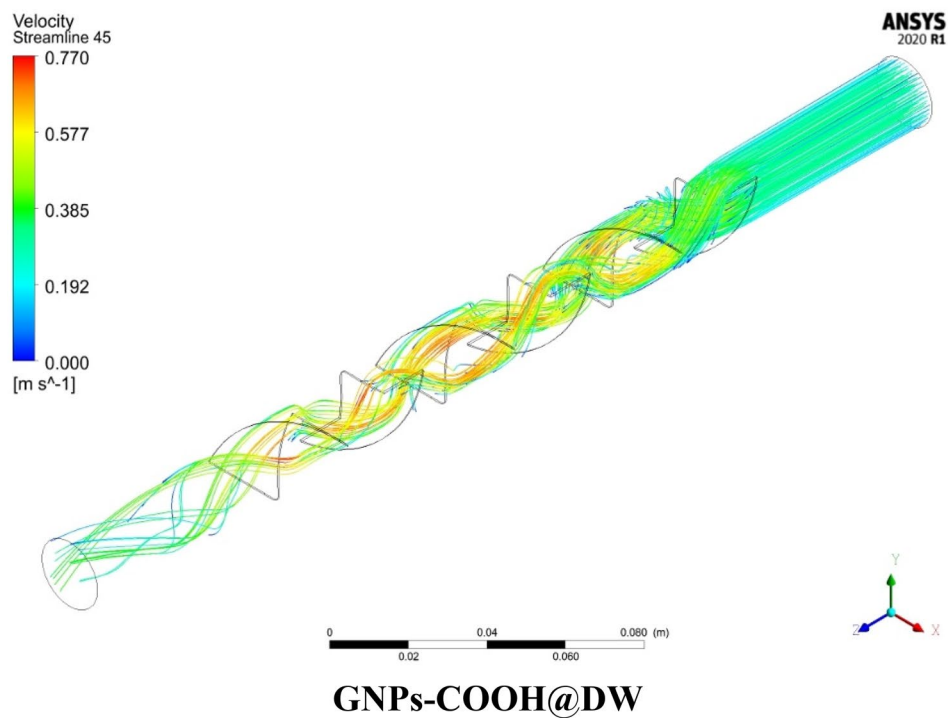
Velocity streamlines of 45° and 90° heat exchangers using DW, 0.1wt.-%-GNPs-SDBS@DW and 0.1wt.-%-GNPs-COOH@DW at $Re = 7000$.

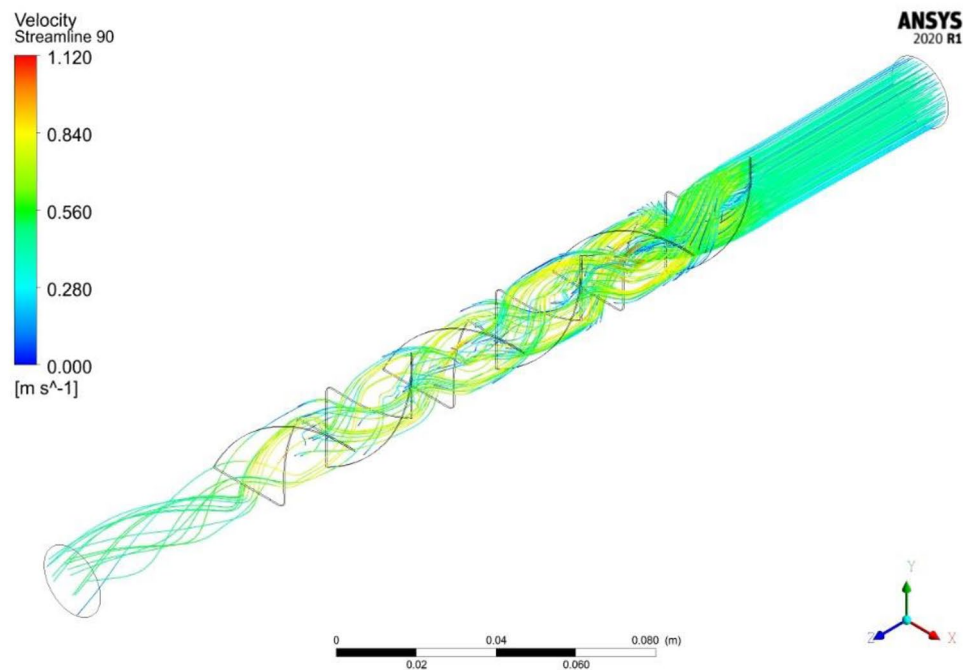


GNPs-SDBS@DW

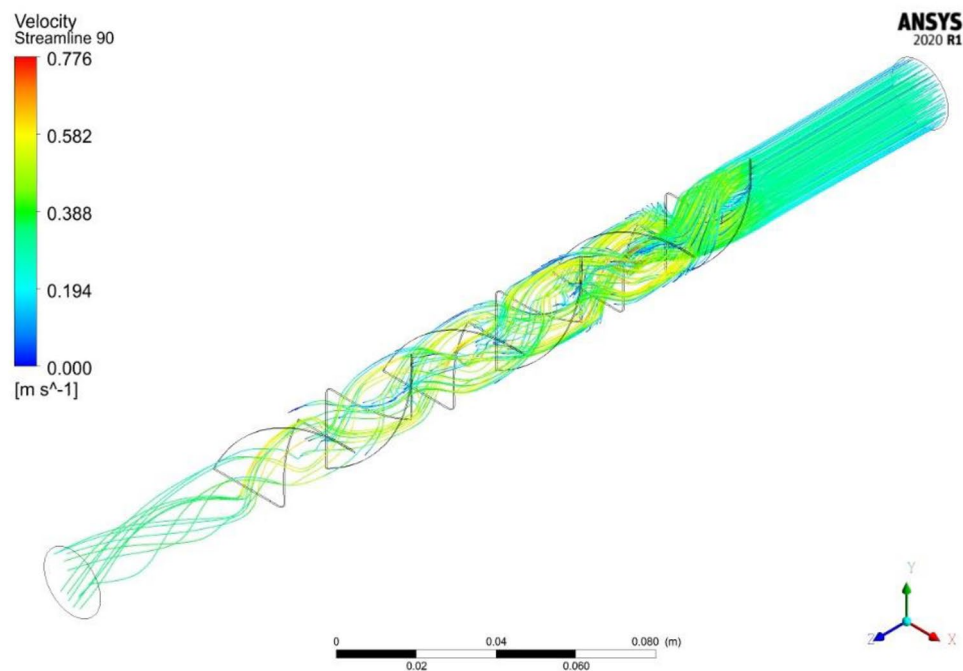


GNPs-COOH@DW





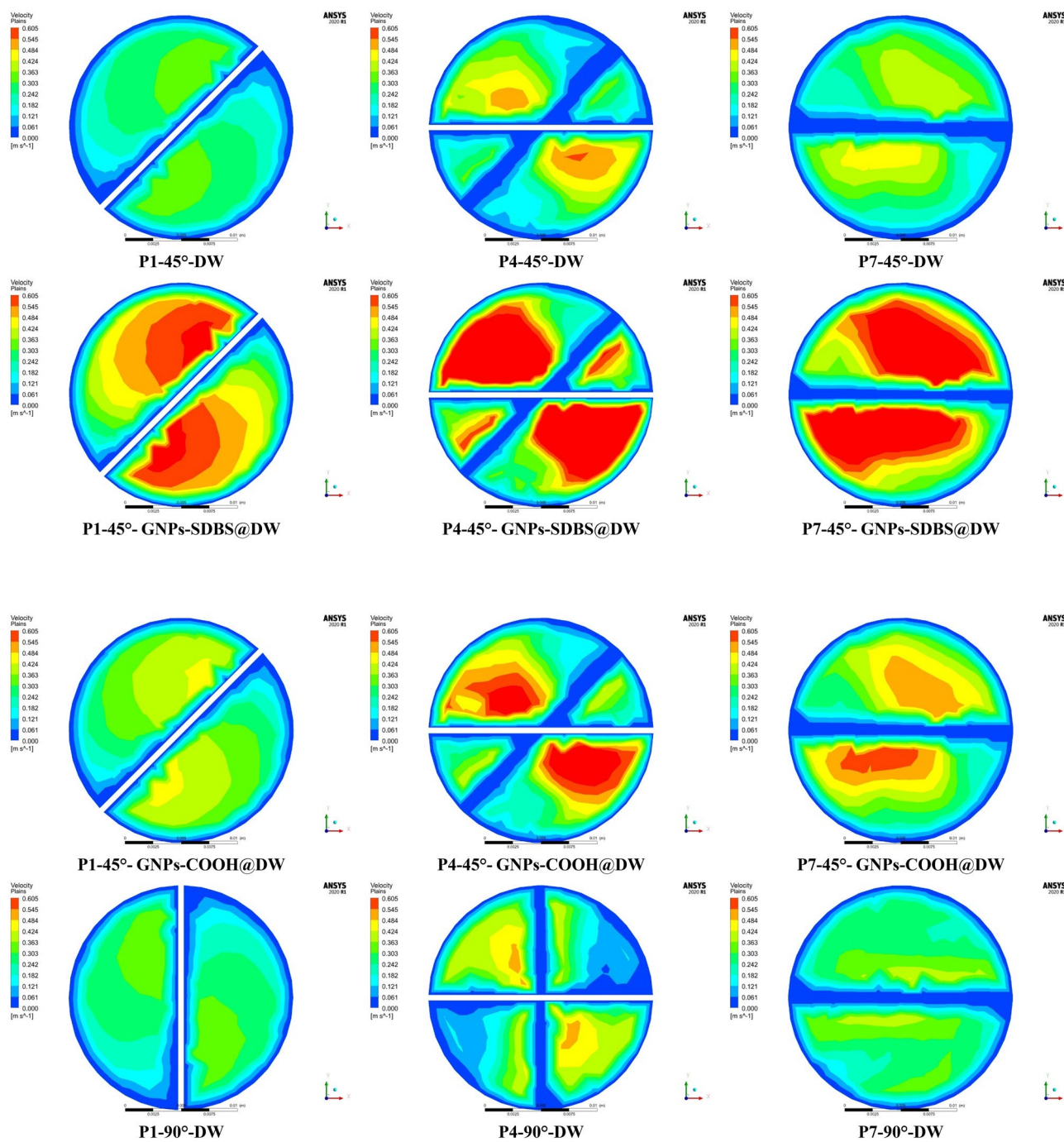
GNPs-SDBS@DW

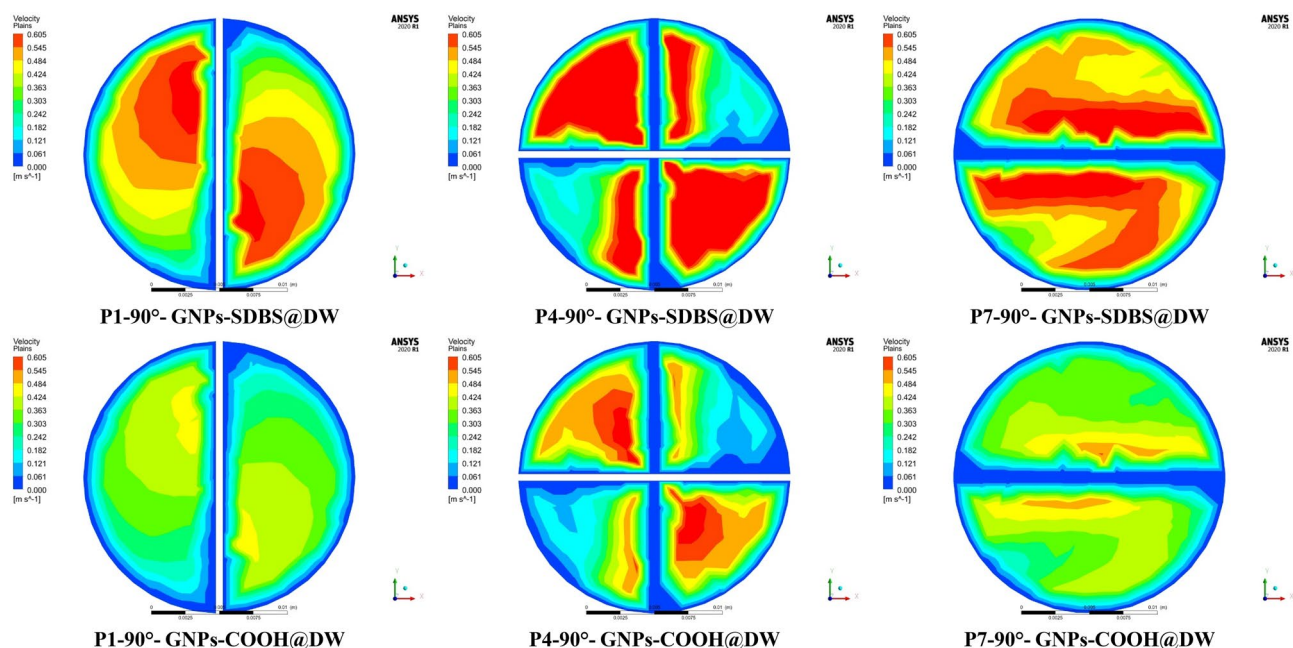


GNPs-COOH@DW

Appendix B

Velocity contours of 45° and 90° heat exchangers using DW, 0.1wt.-%GNPs-SDBS@DW and 0.1wt.-%GNPs-COOH@DW at $Re = 7000$.





Received: 26 August 2022; Accepted: 12 October 2022

Published online: 21 October 2022

References

- Thianpong, C. *et al.* Multi objective optimization of $\text{TiO}_2/\text{water}$ nanofluid flow within a heat exchanger enhanced with loose-fit delta-wing twisted tape inserts. *Int. J. Therm. Sci.* **172**, 107318 (2022).
- Langeroudi, H. G. & Javaherdeh, K. Experimental study of non-Newtonian fluid flow inside the corrugated tube inserted with typical and V-cut twisted tapes. *Heat Mass Transf.* **55**, 937–951 (2019).
- Dong, X. *et al.* Experimental research on heat transfer and flow resistance properties in spiral twisted tube heat exchanger. *Appl. Therm. Eng.* **176**, 115397 (2020).
- Yongsiri, K., Eiamsa-Ard, P., Wongcharee, K. & Eiamsa-Ard, S. J. C. S. Augmented heat transfer in a turbulent channel flow with inclined detached-ribs. *Case Stud. Therm. Eng.* **3**, 1–10 (2014).
- Chamoli, S., Lu, R. & Yu, P. Thermal characteristic of a turbulent flow through a circular tube fitted with perforated vortex generator inserts. *Appl. Therm. Eng.* **121**, 1117–1134 (2017).
- Nakhchi, M. E., Esfahani, J. A. & Kim, K. C. Numerical study of turbulent flow inside heat exchangers using perforated louvered strip inserts. *Int. J. Heat Mass Transf.* **148**, 119143 (2020).
- Fagr, M. H., Rishak, Q. A. & Mushatet, K. S. Performance evaluation of the characteristics of flow and heat transfer in a tube equipped with twisted tapes of new configurations. *Int. J. Therm. Sci.* **153**, 106323 (2020).
- Zeng, M., Ma, T., Sundén, B., Trabia, M. B. & Wang, Q. Effect of lateral fin profiles on stress performance of internally finned tubes in a high temperature heat exchanger. *Appl. Therm. Eng.* **50**, 886–895 (2013).
- Nakhchi, M. E. & Esfahani, J. A. Numerical investigation of heat transfer enhancement inside heat exchanger tubes fitted with perforated hollow cylinders. *Int. J. Therm. Sci.* **147**, 106153 (2020).
- Nuntadusit, C., Wae-Hayee, M., Bunyajitradulya, A. & Eiamsa-Ard, S. Visualization of flow and heat transfer characteristics for swirling impinging jet. *Int. Commun. Heat Mass Transf.* **39**, 640–648 (2012).
- Thianpong, C., Eiamsa-Ard, P., Wongcharee, K. & Eiamsa-Ard, S. Compound heat transfer enhancement of a dimpled tube with a twisted tape swirl generator. *Int. Commun. Heat Mass Transf.* **36**, 698–704 (2009).
- Waqas, H. *et al.* Heat transfer analysis of hybrid nanofluid flow with thermal radiation through a stretching sheet: A comparative study. *Int. Commun. Heat Mass Transf.* **138**, 106303 (2022).
- Waqas, H., Fida, M., Liu, D., Manzoor, U. & Muhammad, T. Numerical simulation of entropy generation for nanofluid with the consequences of thermal radiation and Cattaneo-Christov heat flux model. *Int. Commun. Heat Mass Transf.* **137**, 106293 (2022).
- Khalid, S., Waqas, H., Yasmin, S., Muhammad, T. & Galal, A. M. Hybrid nanofluid to enhance heat transfer with velocity and temperature jump impacts. *Waves Random Complex Med.* **28**, 1–17 (2022).
- Waqas, H. *et al.* Comparative analysis of hybrid nanofluids with Cattaneo-Christov heat flux model: A thermal case study. *Case Stud. Therm. Eng.* **36**, 102212 (2022).
- Hosseinalipour, S. M., Rostami, A. & Shahriari, G. Numerical study of circumferential temperature difference reduction at the absorber tube of parabolic trough direct steam generation collector by inserting a twisted tape in superheated region. *Case Stud. Therm. Eng.* **21**, 100720 (2020).
- Khoshvaght-Aliabadi, M., Davoudi, S. & Dibaei, M. H. Performance of agitated-vessel U tube heat exchanger using spiky twisted tapes and water based metallic nanofluids. *Chem. Eng. Res. Des.* **133**, 26–39 (2018).
- Akyurek, E. F., Geliş, K., Şahin, B. & Manay, E. Experimental analysis for heat transfer of nanofluid with wire coil turbulators in a concentric tube heat exchanger. *Results Phys.* **9**, 376–389 (2018).
- Mirzaei, M. & Azimi, A. Heat transfer and pressure drop characteristics of graphene oxide/water nanofluid in a circular tube fitted with wire coil insert. *Exp. Heat Transf.* **29**, 173–187 (2016).
- Eiamsa-ard, S., Wongcharee, K., Kunarak, K., Kumar, M. & Chuwattabakul, V. Heat transfer enhancement of TiO_2 -water nanofluid flow in dimpled tube with twisted tape insert. *Heat Mass Transf.* **55**, 2987–3001 (2019).

21. He, W. *et al.* Effect of twisted-tape inserts and nanofluid on flow field and heat transfer characteristics in a tube. *Int. Commun. Heat Mass Transf.* **110**, 104440 (2020).
22. Bazdidi-Tehrani, F., Khanmohamadi, S. M. & Vasefi, S. I. Evaluation of turbulent forced convection of non-Newtonian aqueous solution of CMC/CuO nanofluid in a tube with twisted tape inserts. *Adv. Powder Technol.* **31**, 1100–1113 (2020).
23. Naik, M. T., Fahad, S. S., Sundar, L. S. & Singh, M. K. Comparative study on thermal performance of twisted tape and wire coil inserts in turbulent flow using CuO/water nanofluid. *Exp. Therm. Fluid Sci.* **57**, 65–76 (2014).
24. Akhavan-Behabadi, M. A., Shahidi, M., Aligoodarz, M. R. & Ghazvini, M. Experimental investigation on thermo-physical properties and overall performance of MWCNT–water nanofluid flow inside horizontal coiled wire inserted tubes. *Heat Mass Transf.* **53**, 291–304 (2017).
25. Singh, S. K. & Sarkar, J. Improving hydrothermal performance of double-tube heat exchanger with modified twisted tape inserts using hybrid nanofluid. *J. Therm. Anal. Calorim.* **143**, 4287–4298 (2021).
26. Maddah, H. *et al.* Factorial experimental design for the thermal performance of a double pipe heat exchanger using Al₂O₃-TiO₂ hybrid nanofluid. *Int. Commun. Heat Mass Transf.* **97**, 92–102 (2018).
27. Singh, S. K. & Sarkar, J. Experimental hydrothermal characteristics of concentric tube heat exchanger with V-cut twisted tape turbulator using PCM dispersed mono/hybrid nanofluids. *Exp. Heat Transf.* **34**, 1–22 (2020).
28. Bahiraei, M., Mazaheri, N. & Aliee, F. Second law analysis of a hybrid nanofluid in tubes equipped with double twisted tape inserts. *Powder Technol.* **345**, 692–703 (2019).
29. Singh, S. K. & Sarkar, J. Improving hydrothermal performance of hybrid nanofluid in double tube heat exchanger using tapered wire coil turbulator. *Adv. Powder Technol.* **31**, 2092–2100 (2020).
30. Kumar, V. & Sahoo, R. R. 4 E's (Energy, Exergy, Economic, Environmental) performance analysis of air heat exchanger equipped with various twisted turbulator inserts utilizing ternary hybrid nanofluids. *Alex. Eng. J.* **61**, 5033–5050 (2022).
31. Bahiraei, M., Mazaheri, N., Aliee, F. & Safaei, M. R. Thermo-hydraulic performance of a biological nanofluid containing graphene nanoplatelets within a tube enhanced with rotating twisted tape. *Powder Technol.* <https://doi.org/10.1016/j.powtec.2019.07.053> (2019).
32. Onyiriuka, E. J., Obanor, A. I., Mahdavi, M. & Ewim, D. R. E. Evaluation of single-phase, discrete, mixture and combined model of discrete and mixture phases in predicting nanofluid heat transfer characteristics for laminar and turbulent flow regimes. *Adv. Powder Technol.* **29**, 2644–2657 (2018).
33. Sadri, R. *et al.* CFD modeling of turbulent convection heat transfer of nanofluids containing green functionalized graphene nanoplatelets flowing in a horizontal tube: Comparison with experimental data. *J. Mol. Liq.* **269**, 152–159 (2018).
34. Arzani, H. K., Amiri, A., Kazi, S. N., Chew, B. T. & Badarudin, A. Experimental and numerical investigation of thermophysical properties, heat transfer and pressure drop of covalent and noncovalent functionalized graphene nanoplatelet-based water nanofluids in an annular heat exchanger. *Int. Commun. Heat Mass Transf.* **68**, 267–275 (2015).
35. Menter, F. R. Two-equation eddy-viscosity turbulence models for engineering applications. *AIAA J.* **32**, 1598–1605 (1994).
36. Bashtani, I., Esfahani, J. A. & Kim, K. C. Effects of water-aluminum oxide nanofluid on double pipe heat exchanger with gear disc turbulators: A numerical investigation. *J. Taiwan Inst. Chem. Eng.* (2021).
37. Sadri, R. *et al.* A facile, bio-based, novel approach for synthesis of covalently functionalized graphene nanoplatelet nano-coolants toward improved thermo-physical and heat transfer properties. *J. Colloid Interface Sci.* **509**, 140–152 (2018).
38. Hussein, O. A. *et al.* The influence of covalent and non-covalent functionalization of GNP based nanofluids on its thermophysical, rheological and suspension stability properties. *RSC Adv.* **9**, 38576–38589 (2019).
39. Song, Y.-Q., Izadpanahi, N., Fazilati, M. A., Lv, Y.-P. & Toghraie, D. Numerical analysis of flow and heat transfer in an elliptical duct fitted with two rotating twisted tapes. *Int. Commun. Heat Mass Transf.* **125**, 105328 (2021).
40. Li, X. *et al.* Analysis of heat transfer characteristics and entransy evaluation of high viscosity fluid in a novel twisted tube. *Appl. Therm. Eng.* **210**, 118388 (2022).
41. Sundar, L. S., Singh, M. K., Punnaiah, V. & Sousa, A. C. M. Experimental investigation of Al₂O₃/water nanofluids on the effectiveness of solar flat-plate collectors with and without twisted tape inserts. *Renew. Energy* <https://doi.org/10.1016/j.renene.2017.10.056> (2018).
42. Zhang, C. *et al.* A comparative review of self-rotating and stationary twisted tape inserts in heat exchanger. *Renew. Sustain. Energy Rev.* **53**, 433–449 (2016).
43. Khoshvaght-Aliabadi, M. & Eskandari, M. Influence of twist length variations on thermal-hydraulic specifications of twisted-tape inserts in presence of Cu–water nanofluid. *Exp. Therm. Fluid Sci.* **61**, 230–240 (2015).

Acknowledgements

The authors would like to reveal their appreciation and gratitude to the respected reviewers and editors for their constructive comments. In addition, the first author would like to acknowledge the support received from the Nanchang Key Laboratory of Internet of things information visualization technology (Grant No. 2020-NCZDSY-017). Further, the authors thanks the supported received by Al-Mustaqbal University College (Grant number: MUC-E-0122). Finally, an admirable appreciation is keen to the King Fahd University of Petroleum and Minerals, for their technical support.

Author contributions

H.T.: Conceptualization, writing up, analysis, investigation, validation, visualization. O.A.A.: Conceptualization, methodology, data analysis, writing up, analysis, investigation, validation, visualization. O.A.H.: Conceptualization, writing up, analysis, investigation, validation, visualization. W.A.: Conceptualization, writing up, analysis, investigation, validation, visualization. A.H.A.: Conceptualization, writing up, analysis, investigation, validation, visualization. R.Z.H.: Conceptualization, supervision, writing up, analysis, investigation, validation, visualization. M.E.: Conceptualization, writing up, analysis, investigation, validation, visualization. M.W.F.: Writing up, analysis, investigation, validation, visualization. N.A.-A.: Supervision, conceptualization, writing up, analysis, investigation, validation, visualization. Z.M.Y.: Project leader, supervision, conceptualization, writing up, analysis, investigation, validation, visualization.

Competing interests

The authors declare no competing interests.

Additional information

Correspondence and requests for materials should be addressed to Z.M.Y.

Reprints and permissions information is available at www.nature.com/reprints.

Publisher's note Springer Nature remains neutral with regard to jurisdictional claims in published maps and institutional affiliations.



Open Access This article is licensed under a Creative Commons Attribution 4.0 International License, which permits use, sharing, adaptation, distribution and reproduction in any medium or format, as long as you give appropriate credit to the original author(s) and the source, provide a link to the Creative Commons licence, and indicate if changes were made. The images or other third party material in this article are included in the article's Creative Commons licence, unless indicated otherwise in a credit line to the material. If material is not included in the article's Creative Commons licence and your intended use is not permitted by statutory regulation or exceeds the permitted use, you will need to obtain permission directly from the copyright holder. To view a copy of this licence, visit <http://creativecommons.org/licenses/by/4.0/>.

© The Author(s) 2022